JOURNAL OF MATERIALS SCIENCE 31 (1996) 851–860

Characterization of PAN-based carbon fibres with laser Raman spectroscopy

Part I *Effect of processing variables on Raman band profiles*

N. MELANITIS, P. L. TETLOW, C. GALIOTIS*
Materials Department, Queen Mary and Westfield College, London E1 4NS, UK

Laser Raman spectroscopy (LRS) has been employed to characterize the structure and morphology of a series of carbon fibres, to assess the combined effects of ultimate firing temperature (UFT) and pre-graphitization drawing during manufacture and, finally, to investigate the influence of oxidative treatment upon the integrity of the fibre surface. Ten types of PAN-based carbon fibres of varying modulus, diameter and manufacturing method, were examined. All their spectral features were recorded and analysed in terms of position, bandwidth and band intensity. Low-modulus fibres, produced at low graphitization temperatures, exhibit weak and broad Raman bands in the 1200–1700 cm^{-1} frequency region. With the increase of the firing temperature, the spectral features sharpen and new lines appear at higher frequencies. The observed changes in the Raman spectra are discussed in detail and related to alterations in the conditions of manufacture.

1. Introduction

Laser Raman spectroscopy is a very powerful tool for assessing structural differences in carbon fibres [1]. Most of the Raman spectroscopic studies conducted on carbon fibres, have looked at fibres that have been produced by different manufacturers and by different, quite often proprietary, processing routes. As a result of our past collaboration with Courtaulds Graphil plc [2–5], we have conducted a systematic study of the various spectral features of carbon fibres that have been derived from the same precursor (PAN) but by different processing routes. The latter comprised of variable precursor prestretching during the stabilization and/or carbonization stages followed by different degrees of graphitization.

Raman spectroscopy on graphite, carbons and carbon fibres is strongly related to the study of the graphite structure. The lattice dynamics of graphite have been extensively investigated in the past [6] and various force constant models have been developed [7, 8]. The determination of the force constants and, subsequently, the phonon dispersion relations of graphite [9, 10], has allowed the theoretical calculation of the lattice frequencies in each case [9, 11].

Most experimental Raman studies on graphite and carbons cover a Raman frequency range from 0–3300 cm^{-1}. The frequency range up to 1650 cm^{-1} has been denoted as the "first-order" region and from 1650–3300 cm^{-1}, as the "second-order" region. These terms refer to the fundamental and overtone/combination frequencies of the scattering species, respectively [12–14].

A synopsis of the literature [15–29] related to the assignment of the various Raman bands (D, G, D′, G′), is presented in Table I. The letter notation of the Raman bands established in the literature [29] ascribes the 1360 cm^{-1} as the D-line, the 1580 cm^{-1} as the G-line and the remaining 1620, 2720 and 2950 cm^{-1} bands as D′, G′, and G″, respectively. The effect of the polarization [21, 22], the temperature of the laser power [30–35] and the wavelength dependence of the Raman bands has also received some attention in the literature.

2. Experimental procedure

All carbon fibres of this project were supplied by Courtaulds Grafil plc. They can be classified into three general categories, or groups, with respect to their diameter and their manufacturing technology.

Group A consists of three 7 μm diameter fibres produced by a "first generation" technology: acrylic filaments were wet-spun and drawn in hot water and saturated steam to a total draw ratio of 14 times, to yield a final diameter of approximately 12 μm. The filaments were stabilized in hot air until the density had risen to about 1.40 $g\,cm^{-3}$, using a rising-ramped temperature regime (225–245 °C). Primary carbonization was carried out using a maximum temperature of 950 °C, whilst secondary carbonization and graphitization utilized an ultimate firing temperature (UFT) up to 2600 °C, depending on the modulus. No additional drawing processes were carried out. During

* Author to whom correspondence should be addressed.
E-mail: C. Galiotis@QMW.AC.UK

0022–2461

TABLE I The major Raman lines of carbon fibres

	Line			
	D	G	D′	G′
Location (cm^{-1})	1350–1370	1575–1582	~1620	2690–2730
Present in:	poorly graphitized fibres with tendency to disappear at higher graphitization temperatures. Not present in single graphite crystals	single graphite crystal and all carbon fibres	non-graphitized fibres. Strong in low annealing temperatures. Detected as a shoulder of the G-line in higher UFT	crystalline graphite and graphitized fibres. Splits into two at very highly graphitized samples (UFT > 3000 °C). Attenuated in only carbonized fibres
Attributed to:	the breakdown of the lattice symmetry of the graphite cell and assigned to the A_{1g} vibrational mode of the graphite plane, introduced by small crystal size and structural disorder	the vibrational mode E_{2g} of the graphite cell	disorder and small crystallite size. It becomes attenuated when two-dimensional ordering is established and disappears at well-graphitized fibres	overtone of the D-line
References	[15–24]	[14–17]	[18–22]	[14, 19, 20, 26, 27]

TABLE II Manufacturing details for all carbon fibres examined in this work

Fibre	Prestabilization drawing: 245 °C	Stabilization drawing: 270 °C	Carbonization drawing: 950 °C	UFT (°C)
A1	Draw ratio = 14	Constant length	5% shrinkage	2600
A2				1950
A3				1350
B1	Draw ratio = 14	Multi-stage	Constant length	2300
B2				2200
B3				1900
B4				1750
C1	Draw ratio = 14	30% extension	10% shrinkage	2600
C2		20% extension	constant length	2400
C3		10% extension	10% extension	2200

TABLE III Material property values of all carbon examined in this work

Fibre	Diameter (μm)	Young's modulus (GPa)	Tensile strain to failure (%)	Surface treatment[a]
A1	7	390	0.9	0 (No), S
A2	7	305	1.1	S
A3	7	230	1.6	0,S,2×,3×,4×
B1	5	405	1.1	S
B2	5	370	1.3	S
B3	5	335	1.5	S
B4	5	305	1.8	0,B,C,D(= S),E,F
C1	6	378	0.9	S
C2	6	378	1.1	S
C3	6	364	1.1	S

[a]S = Standard treatment, as defined by the manufacturer.
The Young's modulus has been obtained by testing fibre tows up to 0.4% tensile strain.

stabilization, the filaments were held at constant length, whilst during carbonization and graphitization a 5% shrinkage was allowed. The various manufacturing stages for each fibre are displayed in Table II. The three fibres were supplied with and without surface treatment. The degree of surface treatment is indicated for each fibre along with the ultimate fibre modulus in Table III. Fibres A1 and A3 with standard surface treatment are identical to the commercial Courtaulds Grafil fibres HMS and XAS.

Group B consists of four "high-performance" 5 μm diameter fibres, three of which (B1, B2, B3) are laboratory fibres and one (B4) is identical to the commercial Courtaulds Grafil IM 43-750. The latter, in particular,

has been supplied in six different surface treatments, denoted by the letters A(0% treatment), B(5%), C(20%), D(50%), E(100%) and F(200%). 0% stands for the untreated fibre, whilst 50% corresponds to the standard treatment. These fibres differ from the "first generation" fibres in that they were subjected to a multi-stage pre-stabilization drawing [36, 37]. Moreover carbonization and graphitization were carried out with the filaments held at constant length. The manufacturing details and the final material properties are given in Tables II and III.

Group C consists of three fibres, of approximately 6 μm diameter, which possess similar modulus values (Table III) but distinctly different structural morphology. They were prepared so as to illustrate the influence of lateral crystal size development, L_c, and crystallite orientation on the compressive strength of fibres and composites. The lateral growth of graphitic crystals is primarily responsive to the ultimate firing temperature (UFT), whilst crystallite orientation is determined by a combination of drawing (pre-stretching and hot stretching) and UFT. Accordingly, these fibres were produced by varying draw regimes and UFT (Table III) to achieve similar modulus values of approximately 370 ± 10 GPa. The structural parameters for these fibres such as crystallite orientation and crystallite size, are given in Table IV.

To obtain the Raman spectrum of a carbon fibre the specimen was mounted on microscope slides and positioned on the translational experimental stage. The fibre was aligned with its axis parallel to the polarization direction of the incident beam. The laser power on the specimen was approximately 1 mW. A typical exposure time required for spectrum acquisition was 30 s. It should be noted that the penetrating depth of the laser beam is estimated to be about 50 nm [15], which accounts for less than 1% of the fibre diameter.

The effect of the laser power on the Raman spectrum of carbon fibres was studied by increasing the power of the incident laser beam on the specimen from 0.5 mW to 8 mW at discrete steps. Raman spectra from the fibre cross-section were obtained by first embedding the single filaments in a thermoplastic matrix (Cerafix) and, then, by mildly grinding and polishing in the plane normal to the fibre axis [38].

The Raman spectrum was processed using a dedicated software package, assuming Lorentzian distribution for each frequency peak and quadratic distribution for the background.

TABLE IV Structural parameters of Group C carbon fibres

Fibre	Tensile strength (GPa)	Azimuthal full-width at half-maximum,[a] (deg)	Crystallite size, L_c[b] (nm)
C1	4.0	20	6.0
C2	4.1	21	4.4
C3	4.2	22	3.4

[a]The azimuthal full-width at half-maximum, F_{002}, is measured from the X-ray diffraction of the 002 plane.
[b]The crystallite size, L_c, was calculated using Scherrer's equation, assuming that all peak broadening is attributed to crystallite size effect.

3. Results

3.1. The first- and second-order Raman spectrum

The first- and second-order Raman spectrum of all ten carbon fibres examined in this work, are shown in Fig. 1. For comparison purposes, the size of each plot has been normalized to the band of maximum intensity feature.

For both Groups A and B, the fibres produced at the lowest UFT exhibit two broad bands in the first-order region of the Raman spectrum, only. As UFT (and the fibre modulus) increases, the second-order features grow, whistle the first-order bands sharpen and become resolved from each other (Fig. 1). Regarding the fibres of Group C, the increase in the surface crystallinity, as reported in Table IV, results in the consistent enhancement of the G- and G′-lines and the relative reduction of the D-line.

3.2. Closer examination of the major Raman lines

In the spectrum of the high-modulus A1 fibre (Fig. 2), the D′-line accounts only for ~ 10% of the intensity of the G-line, whereas in the intermediate modulus A2 fibre, it rises to about 30% of the G-line, according to the Lorentzian analysis of the spectroscopic data. Furthermore, in the case of the low-modulus fibre A3, the D′-line appears to dominate the fibre spectrum. The two bands (G and D′) have merged in one broad feature, shifting the peak of the band from 1580 cm^{-1} to ~1600 cm^{-1}. The change in the relative intensity is affected both by the rise of the D′-line and the dramatic reduction of the intensity of the graphitic G-line with the decrease in the fibre modulus and fibre surface crystallinity.

Similarly, for the fibres of Group B (Fig. 3), the relative intensity of the D′-line, with respect to the intensity of the G-line, increases from just above 0.2 (B1) fibre to about 0.3 (B3). In the case of the B4 fibre, the "shoulder" D′-line has totally overwhelmed its graphitic counterpart, shifting the peak of the merged (G–D′) feature to ~1600 cm^{-1}.

Finally, for the fibres of group C, the higher the degree of fibre crystallinity, the more intense is the

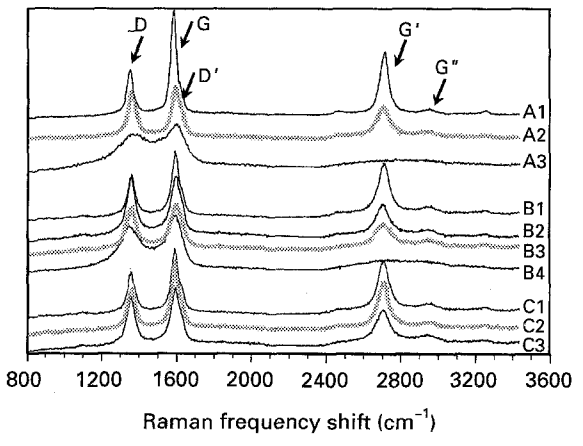

Figure 1 The Raman spectrum of the carbon fibres of this programme of study.

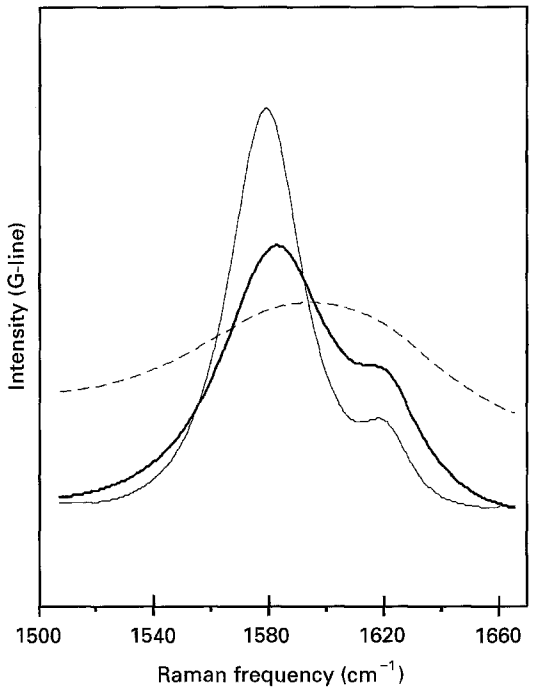

Figure 2 The G-line of the Group A fibres (7 μm diameter, "first generation" fibres). (—) A1, (—) A2, (– – –) A3.

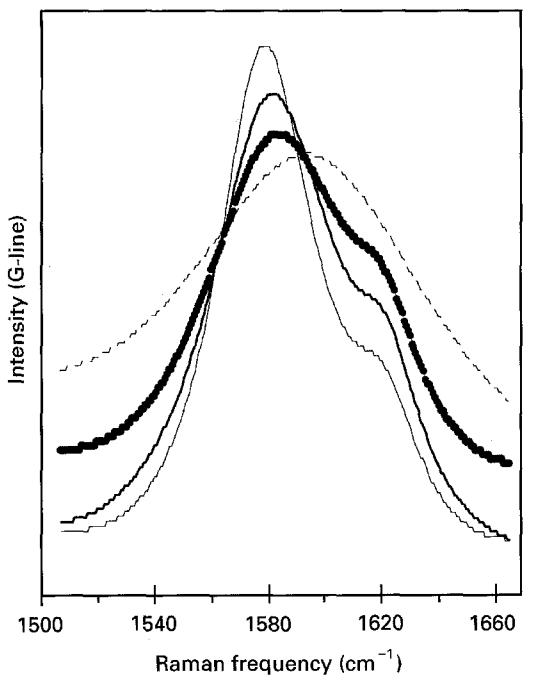

Figure 3 The G-line of the Group B fibres (5 μm diameter, "high-performance" fibres). (—) B1, (—) B2, (●) B3, (– – –) B4.

G-line and, conversely, the weaker is the D′-line of the carbon fibre Raman spectrum (Fig. 4).

High-resolution spectra of the main second-order band (G′-line at ~2700 cm^{-1}) provide evidence for the growth of this feature in tandem to the graphitic G-line for UFT of up to 2600 °C. The higher the fibre modulus and its surface crystallinity, the stronger is the presence of this line in the second-order Raman spectrum of the carbon fibre and the sharper is its linewidth. This is demonstrated in Fig. 5 for the fibres of Group B. Similar plots can be produced for the G′-line of the fibres of Groups A and C.

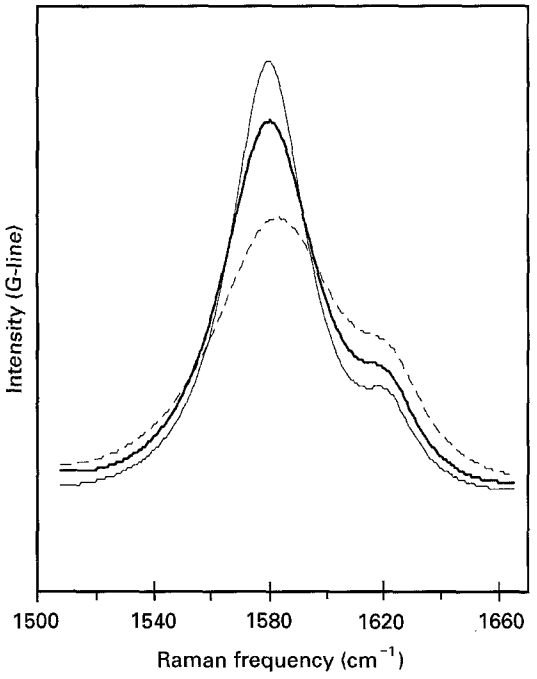

Figure 4 The G-line of the Group C fibres (6 μm diameter, "varying morphology" fibres). (—) C1, (—) C2, (– – –) C3.

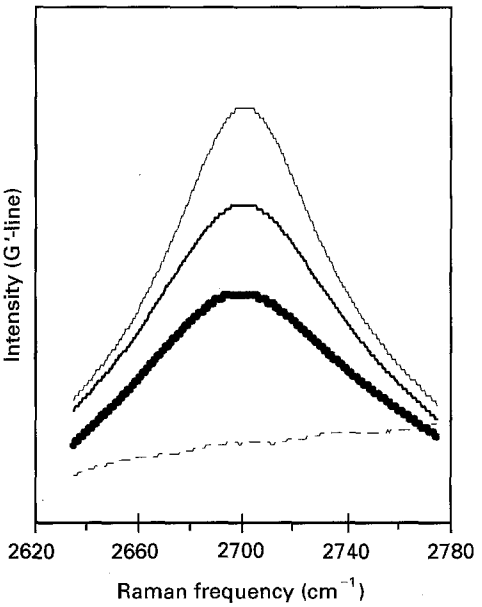

Figure 5 The G′ line of the Group B (5 μm diameter, "high-performance" fibres). (—) B1, (—) B2, (●) B3, (– – –) B4.

3.3. The effect of laser power on the Raman spectrum of carbon fibres

The D-line, the G-line, its "shoulder" D′ and the second-order G′-line of three selected carbon fibres, the A1 (high-modulus 7 μm diameter), the B4 (intermediate modulus 5 μm) and the A3 (low-modulus 7 μm) fibres, have been monitored under varying laser power ranging from 0.5–8 mW on the specimen.

The "disorder"-induced D-line shifts linearly to lower frequencies with increasing laser power, at a rate of $-0.35\ cm^{-1}\ mW^{-1}$ for the A1 fibre, $-0.90\ cm^{-1}\ mW^{-1}$, for the B4, and, $-1.10\ cm^{-1}\ mW^{-1}$, for the A3 carbon fibre. No significant change in the fibres bandwidth is observed within the 0.5–8 mW range.

This is in accordance with recently reported studies [33], in which a measurable increase in the bandwidth of this line was detected only at laser power over 30 mW on the specimen. The effect of laser power on the G-line of the carbon fibre Raman spectrum is negligible with respect to the bandwidth.

A similar trend is followed by all Raman bands, as demonstrated in the summary of Table V. Finally, no change in the relative intensities of the main lines of the Raman spectrum was detected for the three fibres examined, after exposure to a laser power of up to 8 mW.

3.4. The effect of fibre surface treatment on the Raman spectrum of carbon fibres

To study the effect of the surface treatment on the Raman spectrum of carbon fibres, three types of fibres were examined. These were the high-modulus A1 (7 μm) fibre in both its untreated (HMU) and surface-treated (HMS) forms, the intermediate modulus B4 (5 μm) fibre in the untreated (0%) and variously treated forms (5%, 20%, 50%, etc.) and the low-modulus A3 (7 μm) fibre in all of its available surface treatments (Table III).

TABLE V The effect of laser power on the Raman spectrum of carbon fibres

Frequency band	Laser power dependence ($cm^{-1} mW^{-1}$)		
	A1 (390 GPa)	B4 (305 GPa)	A3 (320 GPa)
D	− 0.35	− 0.90	− 1.10
G (or *G–D'*)	− 0.45	− 2.30	− 2.40
D'	− 0.40	–	–
G'	− 0.60	–	–

The first- and second-order Raman spectrum of the treated A1 fibre (Fig. 1) is compared with the spectrum of the untreated fibre, in Fig. 6. The intensity scale is normalized to the intensity of the prominent G-line. The following direct observations can be made for the treated A1 fibre, compared with the untreated one; (a) the "disorder"-induced D-line rises with respect to the G-line, (b) the D'-line becomes more pronounced, and (c) the intensity of the second-order G'-line decreases with respect to the graphitic G-line.

In order to investigate further the effect of oxidative surface treatment upon the Raman spectra of the fibres examined here, the high-resolution real intensity Raman spectra of the treated A1 (HMS) and untreated A1 (HMU) fibres, are superimposed within the range of 1500–1660 cm^{-1} (Fig. 7). The results show that the change in the relative intensities of Fig. 6 is attributed to (a) the increase of the D'-line, and (b) the drop of the G-line.

In contrast to the A1 fibre, the Raman spectrum of the B4 and A3 fibres is not affected by the degree of surface treatment, as demonstrated for the various degrees of surface treatment of the B4 fibre, in Fig. 8.

3.5. The Raman spectrum of the carbon fibre cross-section

Two 7 μm fibres, the A1 and the A3, which correspond to the highest and the lowest modulus fibres of fibre

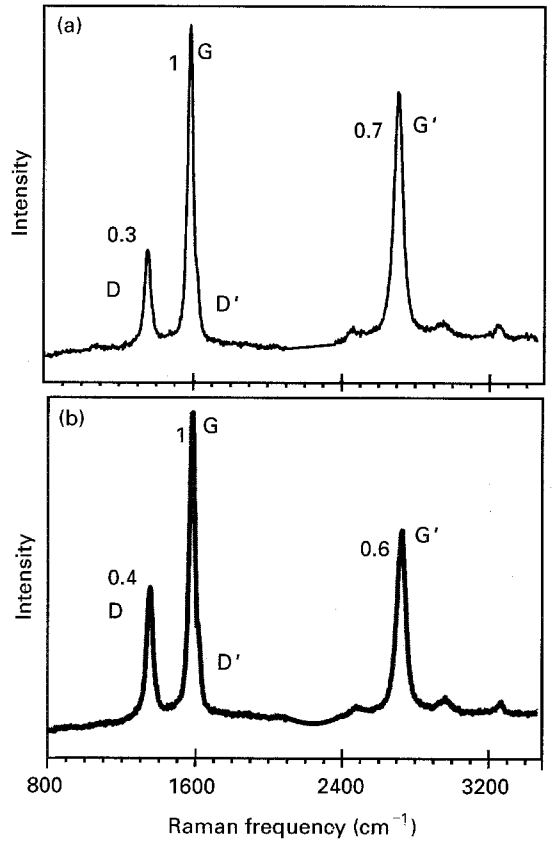

Figure 6 Comparison of the Raman spectrum of (a) the untreated and (b) surface-treated A1 (390 GPa) fibre.

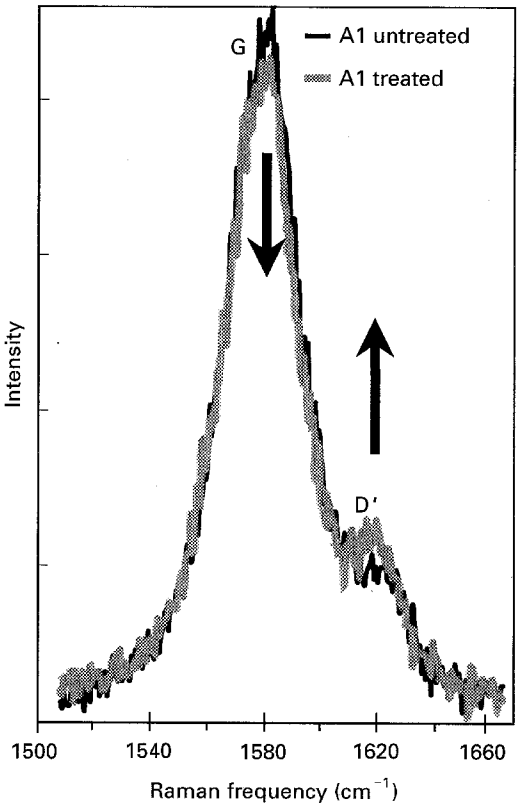

Figure 7 Real intensity high-resolution spectra of the G-line of the untreated and surface treated A1 (390 GPa) fibre.

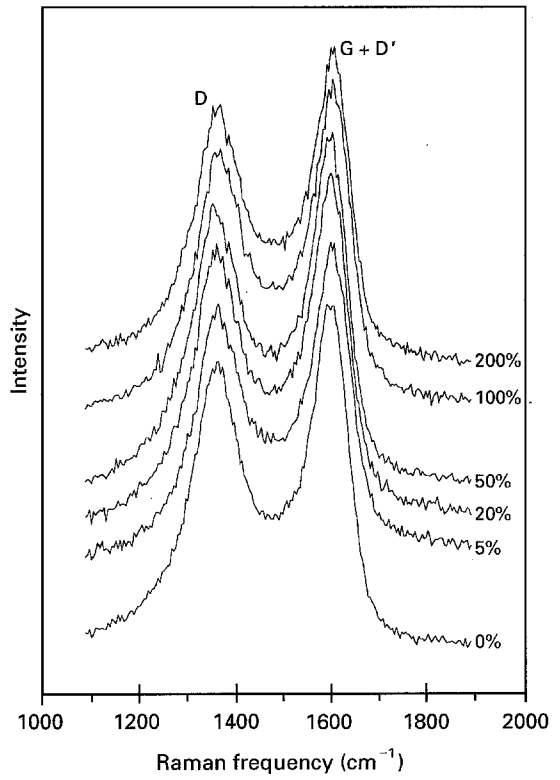

Figure 8 The first-order Raman spectrum of the B4 (305 GPa) fibre for various degrees of surface treatment.

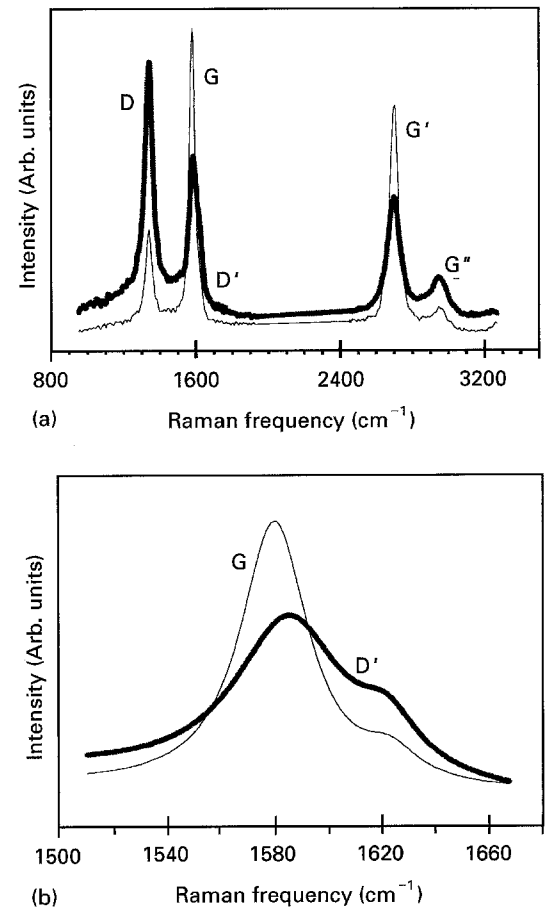

Figure 9 (a) The first-order Raman spectrum taken from (—) the surface and (—) the cross-section of the A1 (390 GPa) fibre (real intensities). (b) High-resolution spectrum (G-line) taken from (—) the surface and (—) the cross-section of the A1 (390 GPa) fibre (normalized intensities).

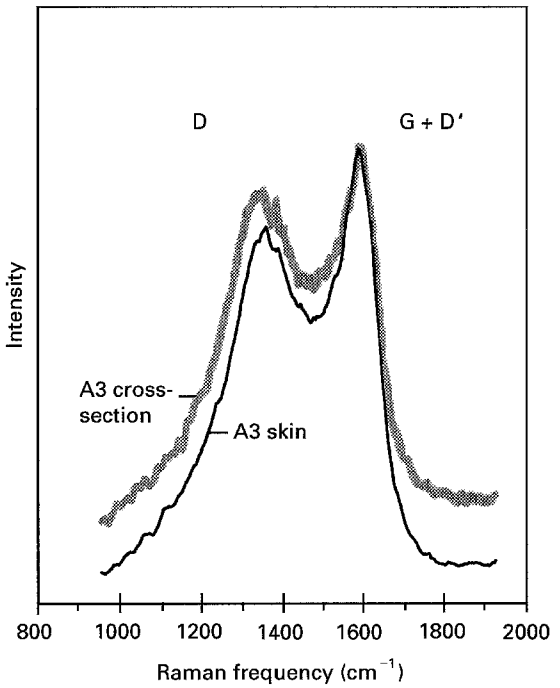

Figure 10 The first-order Raman spectrum taken from the surface and the cross-section of the A3 (230 GPa) fibre (real intensities).

Group A, were selected for preliminary examination. The first- and second-order Raman spectra of the A1 carbon fibre obtained from its cross-section and from the fibre surface, are overlaid in Fig. 9a. The real intensity scaling has been retained. The dramatic rise of the "disorder"-induced features D and D' is accompanied by a sharp reduction of the intensity of the graphitic G-line and the G'-line. The characteristic "crystallinity" ratio, I_D/I_G [15, 16] is increased from a value of 0.35 in the carbon fibre surface Raman spectrum, to a value 1.65 in the cross-sectional Raman spectrum. The enhancement of the 2950 cm^{-1} feature in the cross-section spectrum is consistent with the assignment of this feature as a combination mode of the D and the D'-lines [14]. The high-resolution Raman spectrum near the G-line, presented in Fig. 9b, shows the significant growth of the D' shoulder of the graphitic G-line at the cross-section of the A1 carbon fibre. It should be noted here, that at the fibre cross-section, the incident laser beam "sees" more graphite plane edges than basal planes [22] and, therefore, a reduction in the Raman activity originated from the in-plane vibrational mode, E_{2g}, corresponding to the G-line, is expected.

The first-order Raman spectrum of the low-modulus A3 carbon fibre exhibits almost identical features regardless of whether it originates from the fibre skin or the core (Fig. 10). The intensity ratio, I_D/I_G, increases slightly from 0.80 in the surface spectrum to about 0.9 in the cross-sectional Raman spectrum.

4. Discussion

4.1. The Raman spectrum of carbon fibres

The Raman spectrum of a carbon fibre can provide information about the degree of crystallinity at the

near-surface region of the fibre (~ 50 nm). The sharper the G-line (at 1580 cm^{-1}) and the G′-line (at 2700 cm^{-1}), the higher the surface crystallinity of the fibre and, in general, the fibre Young's modulus. The G-line has been indisputably assigned to the E_{2g} vibrational mode of the graphite cell [14, 15] and is the dominant feature in the spectrum of all fibres tested, with the exception of the low-modulus A3 and the intermediate modulus B4 fibres. In these two cases, the G-line has merged with the "disorder"-induced D′-line at 1620 cm^{-1} (Figs 3 and 4).

As mentioned earlier, the D′-line is related to the "disorder"-induced D-line at $\approx$1360 cm^{-1}. In fact, the intensity ratio between the D′- and D-lines (I_D/I_D) appears to be approximately constant and 0.2–0.3 in value for all the fibres examined. This implies that during carbonization and graphitization both these features grow and subsequently decay at approximately the same rate. Finally, the decrease of the intensity of the second-order G′-line with surface treatment, is again indicative of the close association of this line with the G-line rather than with the D-line [14, 19].

The presence of all "disorder"-induced lines can be derived from the phonon dispersion curves and is due to the distortion of the symmetry of the crystallite and henceforth to the breakdown of the selection rules for Raman activity [11, 19]. In morphological/structural terms, this is a consequence of the presence of crystallites of finite size in non-graphitized carbon fibres [15, 16] and/or the presence of plane edges in the sampling scattering volume which determines Raman activity [22]. Contrary to previous claims [24], both the "disorder" induced D-line and the "graphitic" G-line should be related to the same structural configuration because the full-width at half-maximum (FWHM) of these two bands follow a 1:1 relationship (Fig. 11).

In the case of B4 and A3 fibres, one would expect that the merger of the G and D′-lines would cause a deviation of the ratio of the bandwidths of the D- and G-lines towards lower values. It seems, however, that the broadening of the D-line, possibly due to the presence of residual non-carbon elements, such as nitrogen, exceeds the broadening of the combined G- and D′-lines, hence, the shift to larger values in Fig. 11.

Whichever is the source of these "disorder" features, their presence is an indication of the amount of "graphitic" morphology at the carbon fibre surface. Therefore, in the present investigation, the term "disorder" implies the perturbation of the smoothly stratified long graphite layers by finite-size crystals and/or discontinuities introduced by the graphite plane edges exposed at the surface and near-surface of the fibre. The quality of the graphitic nature of the fibre surface can also be evaluated by the ratio of the intensities of the D- and G-lines, I_D/I_G, known as intensity ratio, or, "crystallinity" ratio.

4.1.1. Effect of oxidative treatment upon the I_D/I_G intensity ratio

The intensity ratio of highly crystalline fibres, such as A1, is not only a function of carbonization and graphitization temperatures, but it also changes with surface

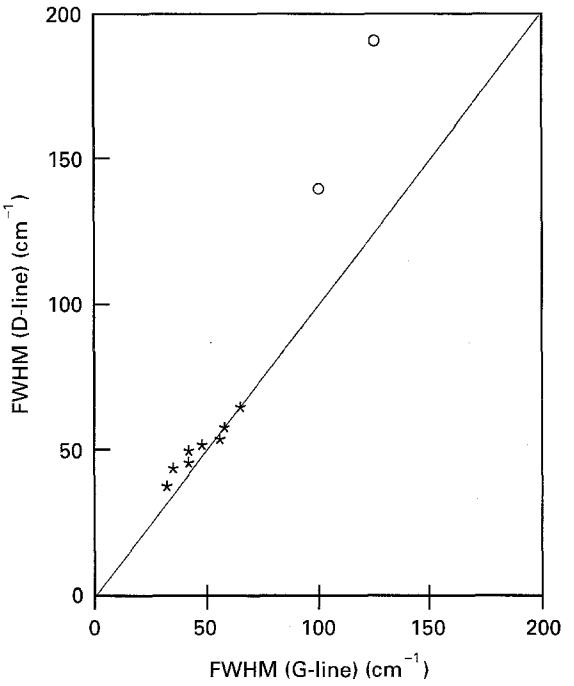

Figure 11 The FWHM of the D-line as a function of the FWHM of the G-line of the carbon fibre Raman spectrum. (—) 1:1 line, (*) experimental (O) A3 and B4.

oxidative treatment. In fact, electron diffraction studies on PAN-based carbon fibres [39] revealed that the crystallite thickness, L_c, and the angle orientation, ϕ, at the skin of heat-treated carbon fibres to 2500 °C, are about 10 nm and 14°, respectively. At the fibre core, values of 33 nm and 24°, respectively, have been obtained. On the other hand, heat-treated carbon fibres at 1500 °C, exhibited L_c = 16 nm and ϕ = 43° in both regions. No change was observed between surface and core of carbon fibres heat treated at 1000 °C [40]. Indeed, as postulated elsewhere [41], the surface treatment on high-modulus carbon fibres removes weak boundary graphite layers from the fibre surface and, consequently, exposes the less crystalline core and a greater number of graphitic edge planes [42–44] to the incident radiation. These findings agree well with the increase of the intensity ratio I_D/I_G with degree of surface treatment, obtained in this work. Similar effects have been observed on the Raman spectrum of Ar^+-etched highly oriented pyrolytic graphite (HOPG) [45]. A schematic representation of the effect of oxidative treatment upon the carbon fibre surface, is shown in Fig. 12.

4.1.2. Effect of skin–core morphology upon the I_D/I_G intensity ratio

The Raman spectroscopic data from carbon fibre cross-sections should be treated with caution before any conclusions are drawn with respect to the internal structure of carbon fibres. As has been shown earlier [46], severe grinding can affect both the graphite interlayer distance and crystallite size, while mild grinding does not induce any damage. The differences in the value of intensity ratio obtained from the surface and the cross-section of the high-modulus A1 fibre, should

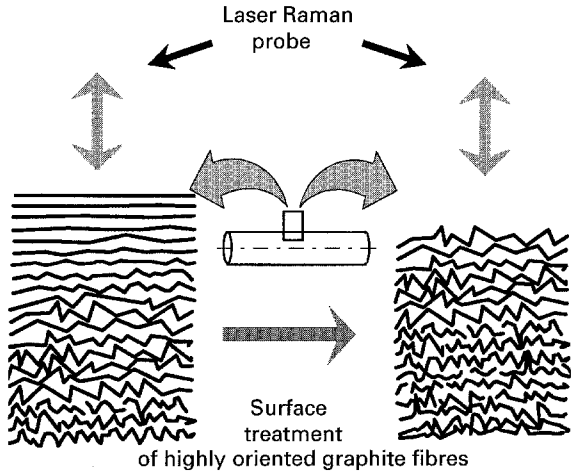

Figure 12 A simple structural model to account for the enhancement of the "disorder"-induced features in the Raman spectrum of surface-treated high-modulus fibres.

not be necessarily interpreted as a skin–core effect because the scattering units are at a different orientation to the incident beam in the two configurations. On the other hand, the surface and cross-section spectra of the B4 and A3 fibres show no significant differences and this indicates the existence of a high degree of structural homogeneity throughout these fibres.

4.1.3. Effect of firing temperature upon the I_D/I_G intensity ratio

Within each fibre group (A and B) all fibres have been produced following a specific temperature and drawing regime. In general, the increase of the UFT, under a constant drawing regime, results in a higher fibre modulus, sharper Raman features and reduction in the intensity ratio I_D/I_G (Fig. 13a, b and c, d). However, in the case of group C fibres which have been manufactured under a variable drawing regime, a reduction of the intensity ratio, I_D/I_G, does not necessarily correspond to a higher modulus fibre (Fig. 13e, f). However, it is worth mentioning again here that the penetration depth is of the order of 50 nm and therefore the intensity ratio I_D/I_G should accurately correlate to the modulus of the near-surface region of the fibre. Fibre drawing (especially hot stretching) during manufacture, tends to orient the crystallites in the direction of the fibre and thus a higher average modulus can be obtained at lower firing temperatures. Therefore, in spite of differences in the "surface" crystallinity and hence "surface" modulus, the average fibre modulus can be kept constant. This has tremendous repercussions for both the compressional behaviour of these fibres but also for the adhesion to polymeric resins. As shown elsewhere [4], a dramatic increase in the compression strength to failure is obtained by producing a high-modulus fibre such as the C3, in which the crystallite size is small but the crystallites are well oriented along the fibre axis by hot drawing during processing. Equally, a fibre which does not exhibit a highly crystalline skin can be surface treated more easily and, at any rate, is expected to adhere better to polymeric resins through mechanical interlocking.

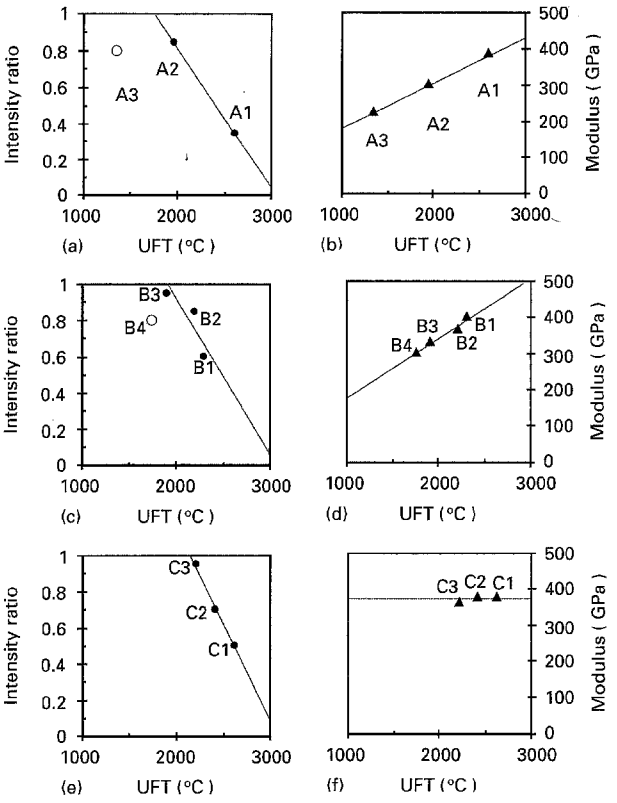

Figure 13 The fibre Young's modulus and the intensity ratio, I_D/I_G, as a function of the UFT for the three groups of fibres examined in this programme of work. (a, b) Group A, (c, d) Group B, (e, f) Group C.

4.2. Special reference to the "poorly" crystalline fibres

The case of the low-modulus A3 and the B4 fibres should be dealt with separately. As mentioned earlier, the Raman features of these two fibres deviate dramatically from the trend followed by the rest of the fibres due to the merger of the G- and the D′-lines (Figs 2 and 3). In addition, the "disorder"-induced D-line, for both the A3 and the B4 fibres, is exceptionally broad. As a result, the plot of the FWHM of these two bands, as a function of the I_D/I_G intensity ratio, deviates considerably from the relationship observed in all other cases (Fig. 14). Furthermore, these two fibres differ from the rest in that they have no second-order Raman features.

Because the Raman spectrum of carbon fibres is related to crystallite symmetry, crystallite size and average orientation [15, 16], the observed differences in A3 and the B4 fibre Raman spectra are indicative of significant structural/morphological differences as compared to the other fibres. It is important to note here that both fibres have been produced at the lowest carbonization temperatures of all fibres in their series. At such low temperatures non-carbon elements are still present in the structure. For example, a nitrogen content of ~3.0% has been measured in fibres carbonized at 1300 °C [40]. Therefore, there may be a critical heat-treatment temperature level, below which, residual nitrogen groups [47], make a significant contribution to the fibre Raman spectrum, particularly if they form heterocyclic compounds [48]. Indeed the Raman spectrum of PAN fibres shown in Fig. 15, exhibits a number of frequency lines in the frequency regions of

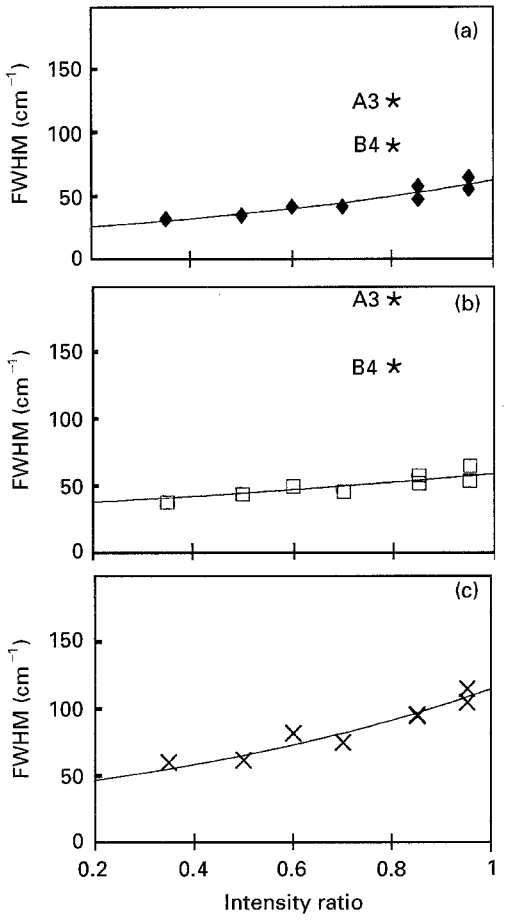

Figure 14 The FWHM as a function of the intensity ratio, I_D/I_G, for the (a) G-line, (b) D-line, and (c) G′-line.

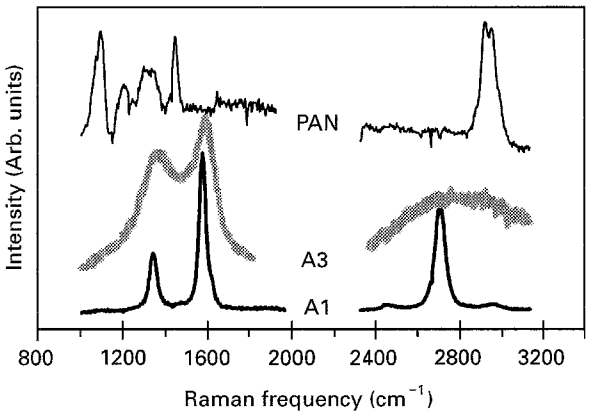

Figure 15 The Raman spectrum of the precursor PAN fibre, compared with the spectra of the A1 (390 GPa) and the A3 (230 GPa) carbon fibres.

1200–1500 and 2950 cm^{-1}, which may still interfere in the spectrum of low-modulus/low heat-treatment carbon fibres. Conclusive evidence for these effects can be produced by monitoring the evolution of the carbon fibre spectrum through all stages of fibre production, such as PAN oxidization, stabilization and graphitization. This work is currently in progress.

4.3. The ambiguous nature of the second-order G′-line

The most pronounced high-frequency line in the Raman spectra of all carbon fibres of this work, with the exception of A3 and B4, is the G′-line appearing at ~2700 cm^{-1}. The FWHM of this line increases as the intensity ratio, I_D/I_G, increases, following the same trend as all major Raman lines (Fig. 14). Moreover, as shown in Fig. 1, the intensity of the G′-line increases proportionally to the intensity of the G-line during graphitization. Although the intensity of this line scales with the intensity of the main "graphitic" G-line, it has been assigned as an overtone of the "disorder"-induced D-line [14] for the following reasons: (a) its frequency value is twice the frequency of the D-line ($2700 = 2 \times 1350$), (b) its FWHM is twice that obtained from the low-frequency bands, and (c) its sensitivity to the excitation wavelength is analogous to that observed for the D-line [34]. Further evidence for the assignment of this band as an overtone is provided by its strain sensitivity, which is over twice as high as that of the low-frequency Raman bands [49].

As mentioned earlier, the G′-line consists of a two-phonon combination and hence requires the existence of a certain degree of structural order in order to be present. Indeed, the development of two-dimensional ordering at higher firing temperatures [27], enhances the intensity of the main G-line at the expense of the D-line, but at the same time allows the evolution of the G′-line. When three-dimensional ordering develops at graphitization temperatures higher than 3000 °C, the D-line disappears completely and the second-order G′-line splits into two bands [27]. Finally, in the single crystal of graphite, only the G-line is present [27].

It appears, therefore, that for non-fully graphitized materials such as carbon fibres, the G′-line is related to the D-line with regards to position and laser wavelength dependence and to the G-line with regards to its intensity. Although, similar effects have been reported by most workers in the field, they have not as yet been fully interpreted or understood.

5. Conclusion

The Raman spectrum of carbon fibres comprises a number of frequency bands, each one assigned to a certain structural configuration. The G-line located at ~1580 cm^{-1}, is assigned to the E_{2g} vibrational mode of the graphite crystal. Fibres produced at low firing temperatures exhibit broad lines (D and D′), which, in some cases, can overshadow the main graphitic G-line. These bands have been attributed to the increase in the amount of the crystallite boundaries due to smaller crystallite size and/or to the presence of graphite plane edge in the fibre structure. The increase in the heat-treatment temperature (firing temperature), yields a fibre product with highly oriented, larger crystallite units, resulting in a higher fibre Young's modulus. The Raman spectrum of such a fibre exhibits a pronounced, narrow and intense G-line, diminishing "disorder" features and an intense high-frequency band at ~2700 cm^{-1} (G′-line). In terms of its Raman frequency value and its wavelength dependence, the G′-line appears as an overtone of the "disorder"-induced D-line; however, in terms of its

other Raman characteristics (intensity, FWHM) is closely associated with the G-line.

The oxidative surface treatment of carbon fibres with highly crystalline surface results in an enhancement of the "disorder" bands of the Raman spectrum. On the contrary, the same treatment has no detectable effect in the Raman spectrum of low modulus and less crystalline fibres. A measure of the fibre surface crystallinity is given by the intensity ratio, I_D/I_G, of the D- and G-lines of the carbon fibre Raman spectrum. However, this ratio cannot be directly related to the bulk fibre modulus, because control of the fibre morphology during manufacture can yield fibres with different intensity ratio, but similar Young's modulus (e.g. fibres C1, C2). The "tailoring" of the fibre morphology can produce a fibre with less "graphitic" surface features, as revealed by its Raman spectrum, but of equal or even higher fibre modulus, e.g. fibres of Group C, or fibres B1 (405 GPa) and A1 (390 GPa). It is believed that as a result of such a morphology alteration (produced by controlled pre-stretching and hot stretching of the precursor and the primer stages fibre), radial anisotropy phenomena can be significantly reduced. Further evidence for this will be presented in Part II [49].

Acknowledgements

This research programme has been supported by funds from the Defence Research Agency (DRA-RAE), the Department of Trade and Industry (DTI), Courtaulds Grafil plc, the Science and Engineering Research Council (SERC) and Queen Mary and Westfield College (QMW). The authors thank Dr M. Pitkethly (DRA-RAE), Dr S. Smith, R. Robinson (Courtaulds plc) and C. K. L. Davies (QMW) for their useful advice, remarks and suggestions.

References

1. M. S. DRESSELHAUS and G. DRESSELHAUS, in "Topics in Applied Physics", Vol. 51, edited by M. Cardona and G. Güntherodt, (Springer, Berlin, 1982) Ch. 2, pp. 3–54.
2. C. GALIOTIS and D. N. BATCHELDER, *J. Mater. Lett.* **7** (1988) 545.
3. N. MELANITIS and C. GALIOTIS, *J. Mater. Sci.* **25** (1990) 5081.
4. *Idem, ibid.* **29** (1994) 786.
5. *Idem, ibid. Proc. R. Soc. Lond.* **440** (1993) 379.
6. A. YOSHIMORI and Y. KITANO, *J. Phys. Soc. Jpn* **11** (1956) 352.
7. M. S. DRESSELHAUS, G. DRESSELHAUS, P. C. ECLUND and D. D. L. CHUNG, *Mater. Sci. Eng.* **31** (1977) 141.
8. A. P. P. NICHOLSON and D. J. BACON, *J. Phys. C Solid State* **10** (1977) 2295.
9. M. MAEDA, Y. KURAMOTO and C. HORIE, *J. Phys. Soc. Jpn* **47** (1979) 337.
10. R. AL-JISHI and G. DRESSELHAUS, *Phys. Rev. B* **26** (1982) 4514.
11. P. LESPADE, R. AL-JISHI and M. S. DRESSELHAUS, *Carbon* **20** (1982) 427.
12. G. TURRELL, "Infrared and Raman Spectra of Crystals" (Academic Press, London, 1972).
13. R. J. NEMANICH, G. LUKOVSKY and S. A. SOLIN, *Solid State Commun.* **23** (1977) 117.
14. R. J. NEMANICH and S. A. SOLIN, *Phys. Rev. B* **20** (1979) 392.
15. F. TUINSTRA and J. KOENIG, *J. Chem. Phys.* **53** (1970) 1126.
16. *Idem, J. Compos. Mater.* **4** (1970) 492.
17. M. NAKAMIZO, R. KAMMERECK and P. L. WALKER, *Carbon* **12** (1974) 259.
18. R. TSU, J. H. GONZALEZ and C. I. HERNANDEZ, *Solid State Commun.* **27** (1978) 507.
19. T. C. CHIEU, M. S. DRESSELHAUS and M. ENDOT, *Am. Phys. Soc.* **26** (1982) 5867.
20. T. P. MENARCH, R. P. COONEY and R. A. JOHNSON, *Carbon* **22** (1984) 39.
21. G. KATAGIRI, H. ISHIDA and A. ISHITANI, in "Proceedings of the 9th Conference on Raman Spectroscopy", Tokyo, edited by ICORS, Tokyo (1984) p. 256.
22. G. KATAGIRI, H. ISHIDA and A. ISHITANI, *Carbon* **26** (1988) 565.
23. E. FITZER, E. GANTNER, F. ROZPLOCH and D. STEINER, *High Temp. High Press.* **19** (1987) 537.
24. E. FITZER and F. ROZPLOCHT, *ibid.* **20** (1988) 449.
25. Y. SASAKI and Y. NISHINA, in "Proceedings of the 9th International Conference on Raman Spectroscopy", Tokyo, edited by ICORS, Tokyo (1984) p. 463.
26. R. LOUDON, *Adv. Phys.* **13** (1964) 423.
27. P. LESPADE, A. MARCHAND, M. COUZI and F. CRUEGE, *Carbon* **22** (1984) 375.
28. R. B. WRIGHT, R. VARMA and D. M. GRUEM, *J. Nucl. Mater.* **63** (1976) 415.
29. R. P. VIDANO, D. B. FISCHBACH, L. J. WILLIS and T. M. LOEHR, *Solid State Commun.* **39** (1981) 341.
30. P. LESPADE, PhD thesis, University of Bourdeaux (1982).
31. A. EBRIL, M. POSTMAN, G. DRESSELHAUS and M. S. DRESSELHAUS, in "Extended Abstracts and Program, 15th Biennial Conference on Carbon", University of Pennsylvania, Philadelphia (1981) 48.
32. R. J. NEMANICH, S. A. SOLIN and D. GYERARD, *Phys. Rev. B* **16** (1977) 2965.
33. D. B. FISCHBACH and M. COUZI, *Carbon* **24** (1984) 365.
34. J. W. AGER, D. K. VEIRS, J. SHAMIR and G. M. ROSENBLATT, *J. Appl. Phys.* **68** (1990) 3598.
35. N. J. EVERALL, J. LUMSDON and D. J. CHRISTOPHER, *Carbon* **29** (1991) 133.
36. M. K. JAIN, M. BALASUBRAMANIAN, P. DESAI and A. S. ABHIRAMAN, *J. Mater. Sci.* **22** (1987) 301.
37. R. T. PEPPER, D. C. NELSON and D. S. LEWING, *UK Pat. Appl.* GB 2084975 (1981).
38. P. L. TETLOW and C. GALIOTIS, *Journal of Materials Science*, to be published.
39. C. BENNET and D. J. JOHNSON, in "Proceedings of the 5th London Carbon and Graphite Conference", Vol. 1 (Soc. Chem. Ind., London, 1978) p. 377.
40. J. B. DONNET and R. P. BANSAL, "*Carbon Fibres*", (Marcel Dekker, New York, 1984).
41. L. T. DRZAL, M. J. RICH and P. F. LLOYD, *J. Adhes.* **16** (1983) 1.
42. I. L. KALNIN and H. JAGER, in "Carbon Fibres and their Composites", edited by E. Fitzer (Springer, Berlin, 1985) p. 62.
43. M. GUIGON, A. OBERLIN and G. DESARMOT, *Fibre Sci. Technol.* **20** (1984) 177.
44. K. J. CHEN and R. J. DIEFENDORF, in "Proceedings of the 16th Biennial Conference on Carbon" (1983) p. 490.
45. H. ISHIDA, H. FUKUDA, G. KATAGIRI and A. ISHITANI, *Appl. Spectrosc.* **40** (1986) 322.
46. M. TIDJANI, J. LACHTER, T. S. KABRE and R. H. BRAGG, *Carbon* **24** (1986) 447.
47. R. M. GILL, "Carbon in Composite Materials", (Plastics Institute, London, 1972).
48. F. R. DOLLISH, W. G. FATELEY and F. F. BENTLEY, "Characteristic Raman Frequencies of Organic Compounds" (Wiley-Interscience, New York, 1974).
49. N. MELANITIS and C. GALIOTIS, *Journal of Materials Science*, to be published.

Received 10 August
and accepted 8 September 1995